Acta Cryst B
STRUCTURAL SCIENCE
CRYSTAL ENGINEERING
MATERIALS
ISSN 2052-5206

Crystal and molecular structure of $[Ni\{2\text{-}H_2NC(=O)C_5H_4N\}_2(H_2O)_2][Ni\{2,6\text{-}(O_2C)_2C_5H_3N\}_2]\cdot 4.67H_2O$; DFT studies on hydrogen bonding energies in the crystal

Mohammad Chahkandi,[a]* Abolfazl Keivanloo Shahrestanaki,[a] Masoud Mirzaei,[b]* Muhammad Nawaz Tahir[c] and Joel T. Mague[d]

[a]Department of Chemistry, Hakim Sabzevari University, Sabzevar, 96179-76487, Iran, [b]Department of Chemistry, Faculty of Science, Ferdowsi University of Mashhad, Mashhad, Khorassan Razavi 917751436, Iran, [c]Department of Physics, University of Sargodha, Sargodha, Pakistan, and [d]Department of Chemistry, Tulane University, New Orleans, LA 70118, USA. *Correspondence e-mail: chahkandimohammad@gmail.com, mirzaeesh@um.ac.ir

Received 27 January 2020
Accepted 14 May 2020

Edited by A. J. Blake, University of Nottingham, England

Keywords: DFT-D; Bader's theory; atoms in molecules; noncovalent interactions; crystal engineering.

CCDC reference: 1891978

Supporting information: this article has supporting information at journals.iucr.org/b

$[Ni\{2\text{-}H_2NC(=O)C_5H_4N\}_2(H_2O)_2][Ni\{2,6\text{-}(O_2C)_2C_5H_3N\}_2]\cdot 4.67H_2O$, a new complex salt containing a bis(2,6-dicarboxypyridine)nickel(II) anion and a bis(2-amidopyridine)diaquanickel(II) cation, was synthesized and characterized. The crystal is stabilized by an extensive network of hydrogen bonds. Alternate layers of anions and cations/water molecules parallel to (010) can be distinguished. Computational studies of the network packing of the title compound by high-level DFT-D/B3LYP calculations indicate stabilization of the networks with conventional and non-conventional intermolecular O—H···O, N—H···O and C—H···O hydrogen bonds along with π-stacking contacts. Due to the presence of water molecules and the importance of forming hydrogen bonds with the involvement of water clusters to the stability of the crystal packing, the importance and role of these water clusters, and the quantitative stability resulting from the formation of hydrogen bonds and possibly other noncovalent bonds such as π-stacking are examined. The binding energies obtained by DFT-D calculations for these contacts indicate that hydrogen bonds, especially O—H···O and N—H···O, control the construction of the crystalline packing. Additionally, the results of Bader's theory of AIM for these interactions agree reasonably well with the calculated energies.

1. Introduction

The field of crystal engineering based on intermolecular interactions tries to design new compounds including organic and metal–organic examples having desired properties such as luminescence (Desiraju, 2003) and magnetism (Tiekink & Vittal, 2006). These functional properties accelerate the development of new useful supramolecular architectures (Carlucci *et al.*, 2003; Lin *et al.*, 2009; He *et al.*, 2008). Biological applications are a significant role of metal–carboxamide complexes (Pandey *et al.*, 2011) with useful properties such as stability, high polarity and conformational diversity making carboxamide species one of the most practical functional groups in organic chemistry (Pattabiraman & Bode, 2011). A promising group of heterocyclic ligands is the pyridine carboxamides which have attracted recent attention because of their role in the preparation of new coordination compounds. They can be utilized in different areas such as epoxidation, hydroxylation, asymmetric catalysis (Belda & Moberg, 2005; Lee *et al.*, 2007), molecular recognition (Kim *et al.*, 2006), anticancer drugs (Patel *et al.*, 2013) and regulation

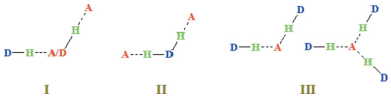

of sirtuin activity (Castro *et al.*, 2011). Some heterocyclic amine and carboxylic acid precursors such as 2,6-diaminopyridine and pyridine-2,6-dicarbonyl dichloride have been used to synthesize ligands such as *N*-(4-methylphenyl)-2-pyridinecarboxamide or its derivatives (Mobin *et al.*, 2015; Kawamoto *et al.*, 1998). These multifunctional ligands bear *O*-, *N*- and *S*-donors which, using noncovalent interactions including hydrogen bonds, π-stacking and different kinds of van der Waals interactions, form diverse supramolecular structures (Deng *et al.*, 2011; Mirzaei, Aghabozorg *et al.*, 2011; Mirzaei, Eshtiagh-Hosseini *et al.*, 2011; Eshtiagh-Hosseini *et al.*, 2010). Recently, co-crystals have gained a lot of attention because of their ability to design and tailor physiochemical properties. Formation of crystalline structures comprising two or more molecular parts through co-crystallization stabilizes the crystal structure by noncovalent contacts (Leroy *et al.*, 2019; Mashhadi *et al.*, 2014). Few examples of binuclear transition metal complexes of pyridine carboxamide are reported; however, there is a growing interest in its derivatives because of the attractive medicinal properties that have been observed (Yeşilkaynak *et al.*, 2017; Lumb *et al.*, 2017; Shi *et al.*, 2010). Coordination compounds with pyridine carboxamide ligands can form crystals with extended π-systems which could provide useful solid state properties Herein, we report a new complex composed of a mononuclear complex cation and a mononuclear complex anion of this limited inventory, namely $[Ni\{2\text{-}H_2NC(=O)C_5H_4N\}_2(H_2O)_2][Ni\{2,6\text{-}(O_2C)_2C_5H_3N\}_2]\cdot 4.67H_2O$, and describe its molecular structure and packing features as well as theoretical calculations to explore the roles of coordinated and uncoordinated water molecules in the construction and stabilization of the supramolecular structure. Those calculations were first performed in the gas phase on the ion pair found in the crystal together with the associated uncoordinated water molecules. No attempt at this stage was made to include a solvent environment. The calculations were designed to explore the crystal packing of ion pairs connected to one another by water molecules. In another set of related calculations, we used the ion pairs by themselves without the uncoordinated water molecules. The results can help to find the role and quantitative influence of water molecules in the stabilization of the crystal packing and the organization of the noncovalent interactions involved, especially hydrogen bonds (HBs).

2. Experimental

2.1. Materials and measurements

All chemicals were analytical A.R grade. Pyridine-2,6-dicarboxylic acid (2,6-pydc) (99%), pyridine-2-carbonitrile (py-2-cbn) (99%), potassium carbonate (99%), hydrogen peroxide (35%), dichloromethane (> 99%), nickel(II) nitrate hexahydrate (99%) and dimethyl sulfoxide (DMSO > 98%) were purchased from Merck Company and used without further purification.

2.2. Synthesis of pyridine-2-carboxamide (py-2-cm)

A solution of py-2-cbn (1.04 g, 10 mmol) in dimethyl sulfoxide (3 ml) in an ice bath (<5°C) was prepared. Then, potassium carbonate (0.2 g) and hydrogen peroxide (1.3 ml, 30%) were added to the solution and the mixture was allowed to reach room temperature. Following this, distilled water (50 ml) was added and after cooling, the product was extracted with dichloromethane. On solvent evaporation the product (py-2-cm) was obtained as a white solid. IR (KBr pellet, cm^{-1}) ν: 3100–3350 (N—H), 1660 $(C{=}O)_{carboxamide}$. M.p. 180°C (Fig. 1S).

2.3. Synthesis of (py-2-cm)$_2$(2,6-pydc)

A solution of 2,6-pydc (167 mg, 1 mmol) in distilled water (10 ml) was added to a solution of py-2-cm (224 mg, 2 mmol) in distilled water (10 ml). The mixture was stirred for 30 min at 90°C and then cooled to room temperature. During slow evaporation of the solvent at room temperature, fine needle-like colorless crystals of the product were obtained after one week. Yield: 57% (based on 2.6-pydc). Anal. Calcd for $C_{19}H_{17}N_5O_6$: C, 53.35; H, 3.97; N, 19.89%. Found: C, 53.24; H, 4.01; N, 19.73%. IR (KBr pellet, cm^{-1}) ν: 2480 and 2870 (O—H), 1710 $(C{=}O)_{carboxylate}$, 1660 $(C{=}O)_{carboxamide}$, 1310, 1260 (C—OH). M.p. 180°C (Fig. 1S).

2.4. Synthesis of [Ni(py-2-cm)$_2$(H$_2$O)$_2$][Ni(2,6-pydc)$_2$]·4.67H$_2$O (1W)

A solution of (py-2-cm)$_2$(2,6-pydc) (411 mg, 1 mmol) in distilled water (20 ml) was added to a solution of $Ni(NO_3)_2\cdot 6H_2O$ (120 mg, 0.5 mmol) in distilled water (5 ml). The resulting blue–green solution was stirred at 90°C for one hour and cooled to room temperature. During slow evaporation of the solvent at room temperature, small cubic blue–green crystals of **1W** were obtained after five days. Yield: 63% (based on Ni). Anal. Calcd for $C_{26}H_{31.50}N_6Ni_2O_{16.75}$ (813.49): C, 38.35; H, 3.87; N, 10.32%. Found: C, 38.30; H, 3.98; N, 10.27%. IR (KBr pellet, cm^{-1}) ν: 2870, 2480 (O—H), 1710 $(C{=}O)_{carboxylate}$, 1660 $(C{=}O)_{carboxamide}$, 1310, 1260 (C—OH). M.p. 255°C.

2.5. X-ray diffraction experimental details

X-ray data were collected at 296 K on a Bruker Kappa APEX II CCD diffractometer equipped with a graphite monochromator and a sealed molybdenum tube (λ = 0.71073 Å). The raw data were converted to F^2 values with *SAINT* (Bruker, 2016) while multiple measurements of equivalent reflections provided the basis for an empirical absorption correction as well as a correction for any crystal deterioration during the data collection (*SADABS*; Bruker, 2016). The structure was solved by direct methods and refined by full-matrix least-squares procedures using the *SHELXTL* program package (Bruker, 2016). Hydrogen atoms attached to carbon in the cation and anion were included as riding contributions in idealized positions with isotropic displacement parameters tied to those of the attached atoms. Those

Table 1
Experimental details for **1W**.

Crystal data	
Chemical formula	$C_{26}H_{31.34}N_6Ni_2O_{16.67}$
M_r	813.49
Crystal system, space group	Triclinic, $P\overline{1}$
Temperature (K)	296
a, b, c (Å)	10.1294 (7), 12.2011 (9), 14.2430 (11)
α, β, γ (°)	82.035 (4), 74.232 (3), 79.373 (3)
V (Å^3)	1657.7 (2)
Z	2
$F(000)$	839
D_x (Mg m^{-3})	1.627
Radiation type	Mo $K\alpha$
No. of reflections for cell measurement	5643
μ (mm^{-1})	1.22
Crystal size (mm)	0.38 × 0.20 × 0.18
Data collection	
Diffractometer	Bruker Kappa APEXII CCD
Absorption correction	Multi-scan (*SADABS*; Bruker, 2016)
T_{min}, T_{max}	0.640, 0.840
No. of measured, independent and observed [$I > 2\sigma(I)$] reflections	20 962, 7584, 5642
R_{int}	0.047
(sin $\theta/\lambda)_{max}$ (Å^{-1})	0.650
Refinement	
$R[F^2 > 2\sigma(F^2)]$, $wR(F^2)$, S	0.041, 0.113, 1.03
No. of reflections	7584
No. of parameters	515
No. of restraints	18
H-atom treatment	H atoms treated by a mixture of independent and constrained refinement
$\Delta\rho_{max}$, $\Delta\rho_{min}$ (e Å^{-3})	0.64, −0.34

Computer programs: *APEX2* (Bruker, 2016), *SAINT* (Bruker, 2016), *SHELXS97* (Sheldrick, 2008), *SHELXL2014/6* (Sheldrick, 2015), *ORTEP-3 for Windows* (Farrugia, 1997) and *PLATON* (Spek, 2020), *WinGX* (Farrugia, 1999) and *PLATON* (Spek, 2020).

attached to oxygen and to nitrogen were placed in locations derived from a difference map. Their coordinates were refined but their displacement parameters were tied to those of the attached atoms. Satisfactory hydrogen bond parameters were achieved with this model. The *PLATON* software (Spek, 2020) was used to calculate bond distances, bond angles, torsion angles, hydrogen bond and other geometric parameters. The *Mercury3.7* software (Macrae *et al.*, 2006) was used to generate the figures and to perform other calculations. The crystal data and refinement of the title compound are given in Table 1. For more information, see Section 3.1 and Figs. 1, 2, 3 and 4.

2.6. Computational procedure

All calculations have been performed at the B3LYP level of the DFT method with LANL2DZ for Ni and 6-311+G(d,p) basis sets for other atoms in the *Gaussian09* program (Frisch *et al.*, 2009). For evaluation of the energies of the noncovalent interactions and the total stabilization energy of the respective network, the following procedure was followed. First, the geometry of [Ni(py-2-cm)$_2$(H$_2$O)$_2$][Ni(2,6-pydc)$_2$] (**1-mon**),

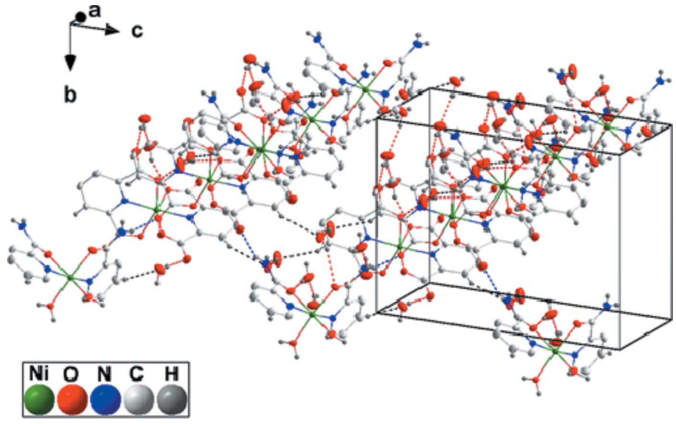

Figure 1
Perspective view of **1W** with labeling scheme and 30% probability ellipsoids. Hydrogen bonds are shown by dashed lines.

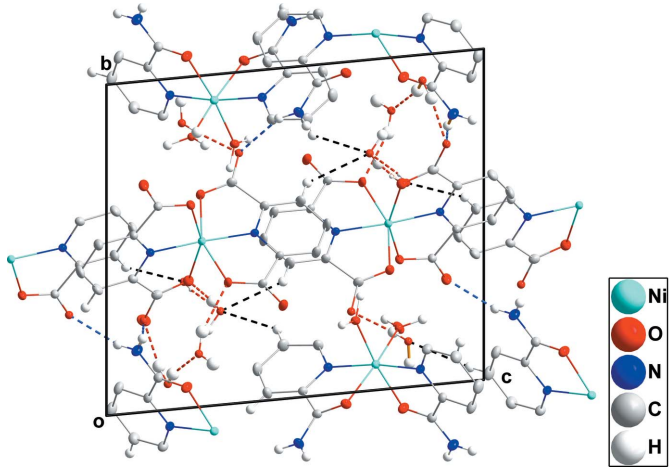

Figure 2
A portion of the basic building block of the crystal of **1W**. The O—H···O and N—H···O hydrogen bonds are shown, respectively, by red and blue dashed lines.

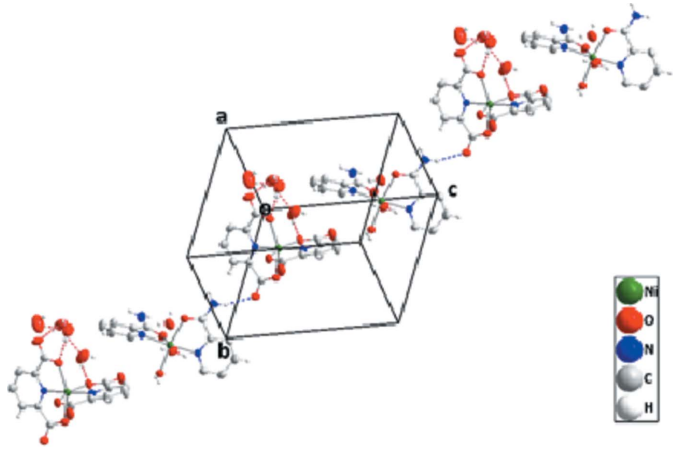

Figure 3
Side view of one layer in the crystal of **1W** generated by N—H···O (blue dashed lines) and O—H···O (red dashed lines) hydrogen bonds.

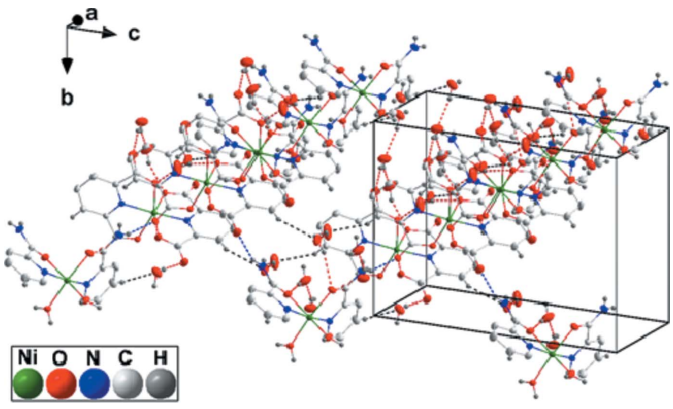

Figure 4
Portions of two layers in the crystal of **1W** showing the connections between them. Intermolecular interactions are depicted as in Fig. 3.

and $[Ni(py\text{-}2\text{-}cm)_2(H_2O)_2][Ni(2,6\text{-}pydc)_2]\cdot 2H_2O$ **(1W-mon)** monomers as the smallest independent units were full optimized, separately (see Fig. 5). Then, for evaluation of the noncovalent contacts in the crystalline network, the crystal packing of each monomer as a cluster network (**1-CN**) and a water cluster network **(1-WCN)** were respectively selected and frequency calculations were performed (see Figs. 6, 7, 8 and 9 and Section 3.3). The atomic positional coordinates taken from the X-ray structure were used in the preparation of the initial unoptimized **1-WCN** as well as for the **1-CN** network. For this purpose, the initial **1-WCN** was optimized and then from the optimized structure, the uncoordinated water molecules were removed and this new structure was reoptimized as the **1-CN** network. Following this, the noncovalent interactions that stabilized these networks were determined. The computed energies of those interactions using the

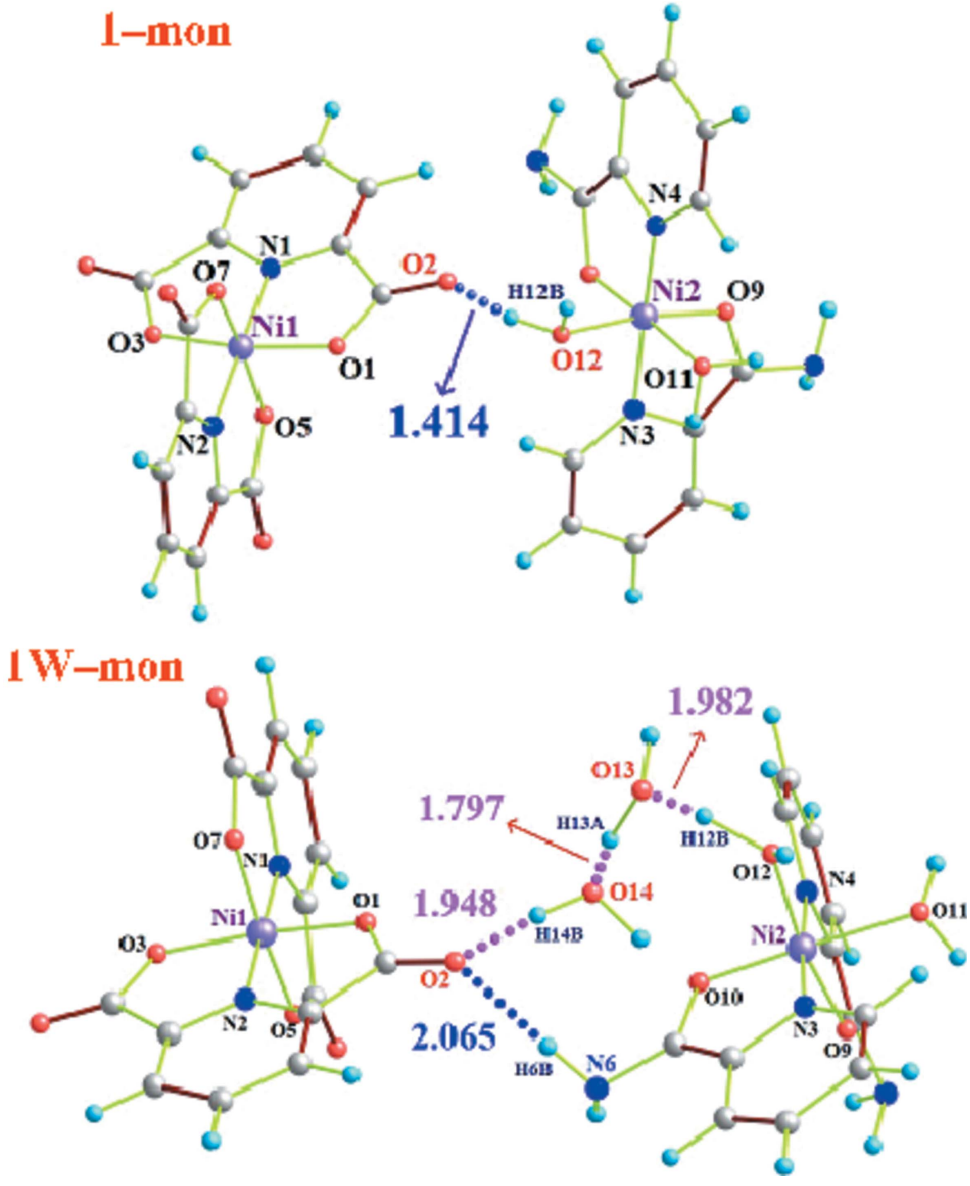

Figure 5
Optimized B3LYP/LANL2DZ/6-311+G(d,p) structures of **1-mon** and **1W-mon**. The dotted lines with distances in Å show intermolecular hydrogen bonds.

B3LYP-D (Jurečka *et al.*, 2007) functional were corrected for basis set superposition error (Boys & Bernardi, 1970). Selected experimental and theoretical geometrical parameters of **1-mon** are listed in Table 2. Also, the geometrical parameters of the hydrogen bond and all involved noncovalent interactions and their related binding energies for **1-CN** and **1-WCN** are summarized in Table 1S. Finally, calculations of 'atoms in molecules' (AIM) within Bader's theory (Bader, 1990, 1985, 1991) were performed for better analysis of related noncovalent contacts at the same applied level of theory. The AIM results obtained for **1-CN** and **1-WCN** are illustrated by the *AIMAll* program (Todd & Keith, 2010) in Figs. 2S and 3S and Tables 3 and 4.

3. Results and discussion

3.1. Crystal and molecular structure of 1W

Table 1 shows the pertinent crystallographic data for **1W**. Since all dimensions of the best crystals obtained were less than 0.1 mm none were found to diffract very strongly so even with the longest reasonable exposure times the best resolution

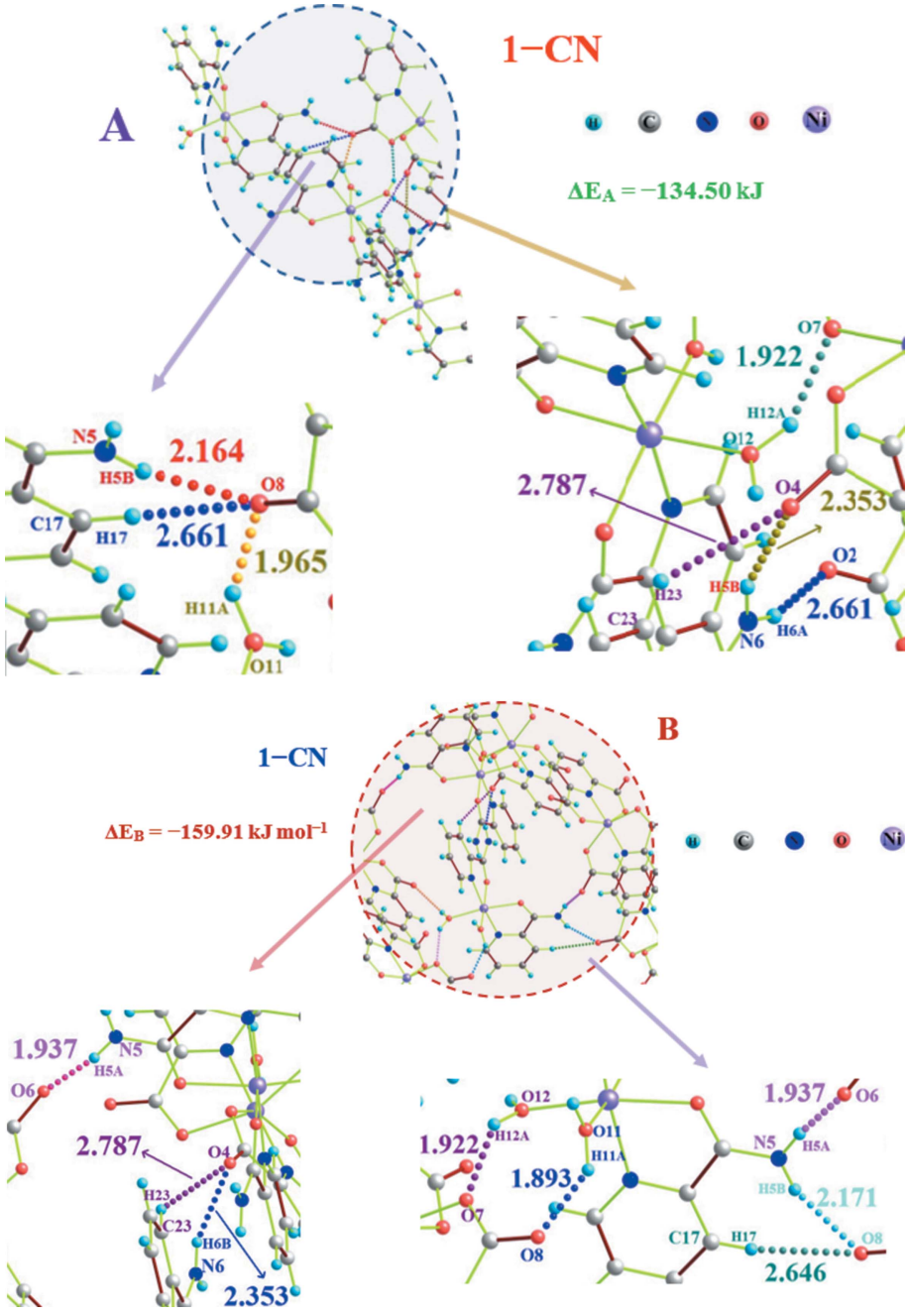

Figure 6
The optimized structure of the **1-CN**. For more clarity the involved hydrogen bonds are shown in two separated parts A and B. Distances are shown in Å.

obtained was 1.0 Å. Selected bond distances and interbond angles of **1W** are collected in Table 2 while hydrogen bonds are presented in Table 1S. The asymmetric unit of the title compound is a neutral ion pair plus uncoordinated water molecules of overall formula $C_{26}H_{31.34}N_6Ni_2O_{16.67}$ and molecular weight of 811.97 g mol^{-1} that crystallizes in the triclinic space group $P\overline{1}$. Both cation and anion are six-coordinate mononuclear nickel complexes, the cation having **pycm** and water as ligands and the anion coordinated by **pydc** ligands. In the anion (**1W-pydc**), the Ni^{II} center is bonded to the carboxylate groups and the nitrogen atoms of two **pydc** ligands while for the cation (**1W-pycm**), the ring nitrogen and the oxygen of the amide group of each of the two **pycm** ligands and two water molecules are coordinated to the metal center (Fig. 1). In the cation, the **pycm** ligands form five-membered chelate rings in which the intraligand angles are constrained by the ligand geometry so that with the two monodentate water ligands, the coordination sphere is moderately distorted from regular octahedral. Thus, the angles about Ni2, with the exception of the two intraligand angles N3—Ni2—O9 [79.60 (7)°] and N4—Ni2—O10 [78.81 (7)°], do not deviate from the ideal values of 90 and 180° by much more than 10°. In the anion, the constraints of the tridentate **pydc** ligands lead to significantly greater distortions. Thus the angles between *cis*-disposed donor atoms range from 76.99 (7)° (N1—Ni1—O1) to 106.11 (7)° (N2—Ni1—O3) while the *trans* angles O1—Ni1—O3 and O5—Ni1—O7 are, respectively, 155.18 (7) and 155.21 (7)°. The dihedral angle between the two pyridine rings of the pydc ligands is 84.44 (13)°.

In the crystal, the cation–anion pairs are connected by N5—H5*B*···O8 hydrogen bonds and, with the uncoordinated water molecules hydrogen bonded to the anion, line up approximately parallel to (111) (Fig. 2).

These groupings are linked into layers approximately parallel to (111) by O11—H11*A*···O8, O12—H12*A*···O7, O13—H13*A*···O5, O14—H14*A*···O17, O14—H14*B*···O6, O15—H15*B*···O13 and O17—H17*B*···O1 hydrogen bonds (Fig. 3).

3.1.1. Database survey. A search of the Cambridge Structural Database (Version 2.0.4, updated to March 2020; Groom *et al.*, 2016) located 55 structures containing the anion Ni[(*L*3)$_2$]$^{2-}$ where *L*3 is pydc or related ligands also containing a hydroxyl or carboxylate group at the 4-position of the pyridine ring. Of these, 12 also contain an Ni^{II} cation such as [Ni(en)$_3$]$^{2+}$ (en = 1,2-diaminoethane) (CIKSOE; du Preez *et al.*, 1984), [Ni(phen)$_3$]$^{2+}$ (phen = 1,10-phenanthroline) (FAFHUR; Tin *et al.*, 2007) or [Ni(*L*2)(H$_2$O)$_4$]$^{2+}$ [*L*2 = 4-(2-amino-1,3-thiazol-4-yl)-1,3-thiazol-2-amine] (GOLPIH; Liu *et al.*, 2009). The remaining nine structures are FAFGAW (McMurtrie & Dance, 2010), FAMKIP (Tabatabaee *et al.*, 2012*a*), KEMWOC (Tabatabaee *et al.*, 2012*b*), OWUFUJ (Jerome *et al.*, 2016), QOCPAA (Kirillova *et al.*, 2008), SAVXUL (Soleimannejad *et al.*, 2017), TICJEV (Park *et al.*, 2007), VENHIG (Zhang *et al.*, 2006) and WURBUH (Eshtiagh-Hosseini *et al.*, 2010). In all of these, the two Ni(ONO) coordination planes are nearly perpendicular (dihedral angle 86.3–90.0°) with the plane defined by the pyridine ring and the two attached carboxyl carbon atoms inclined to the Ni(ONO) coordination plane by 0–8.4°. More often than not this angle is different for the two ligands in a given anion. The intraligand O—Ni—O angles range from 154.9 (5)° to 156.5 (4)° although in the majority of the struc-

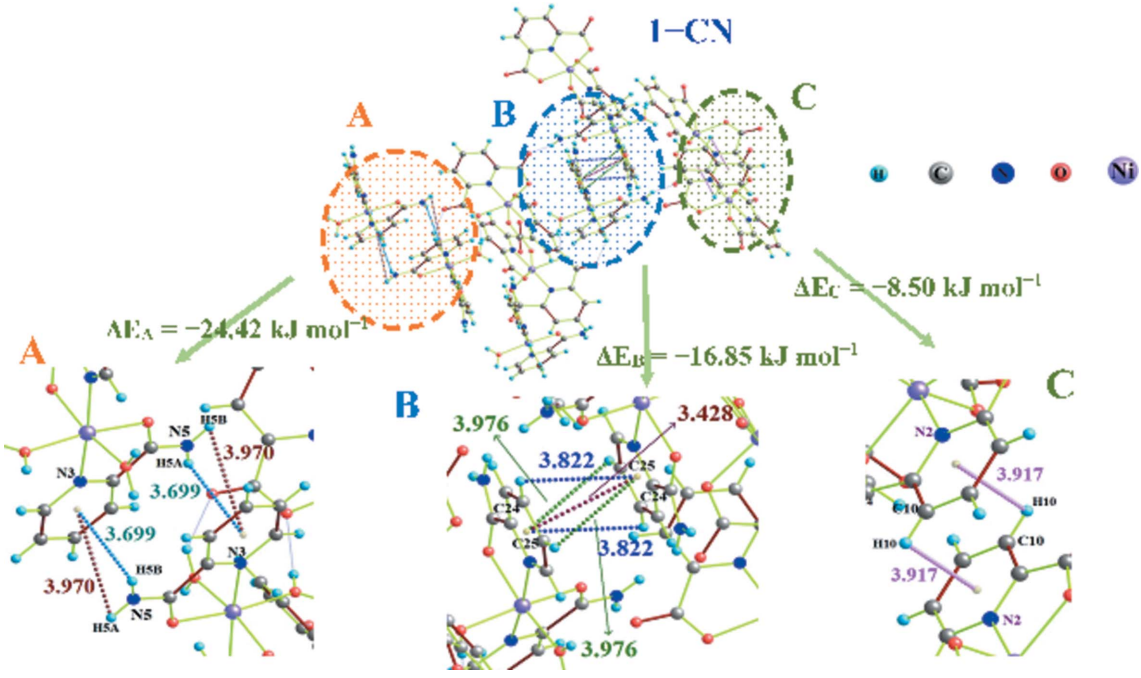

Figure 7
The optimized **1-CN** constructed by stacking interactions. For more clarity the involved interactions are shown in three separated parts A, B, and C. Distances are shown in Å.

tures they are closer to 155.5° and close to equal within experimental error. The N—Ni—N angles are in the range 172.35 (12) to 179.13 (13)° while the Ni—O distances are all around 2.1–2.2 Å and the Ni—N distances are shorter at around 1.95 Å. Inspection of Table 2 indicates that the relevant bond distances and interbond angles of the anion in the present work are comparable with those in the literature. Moreover, the dihedral angle between the two Ni(ONO) coordination planes is 87.5° while the 'fold' of the ligand as defined above is 5.2° for one ligand and 3.7° in the other, again a similar situation to what appears in the literature. Due to the considerable differences in size, shape and hydrogen-

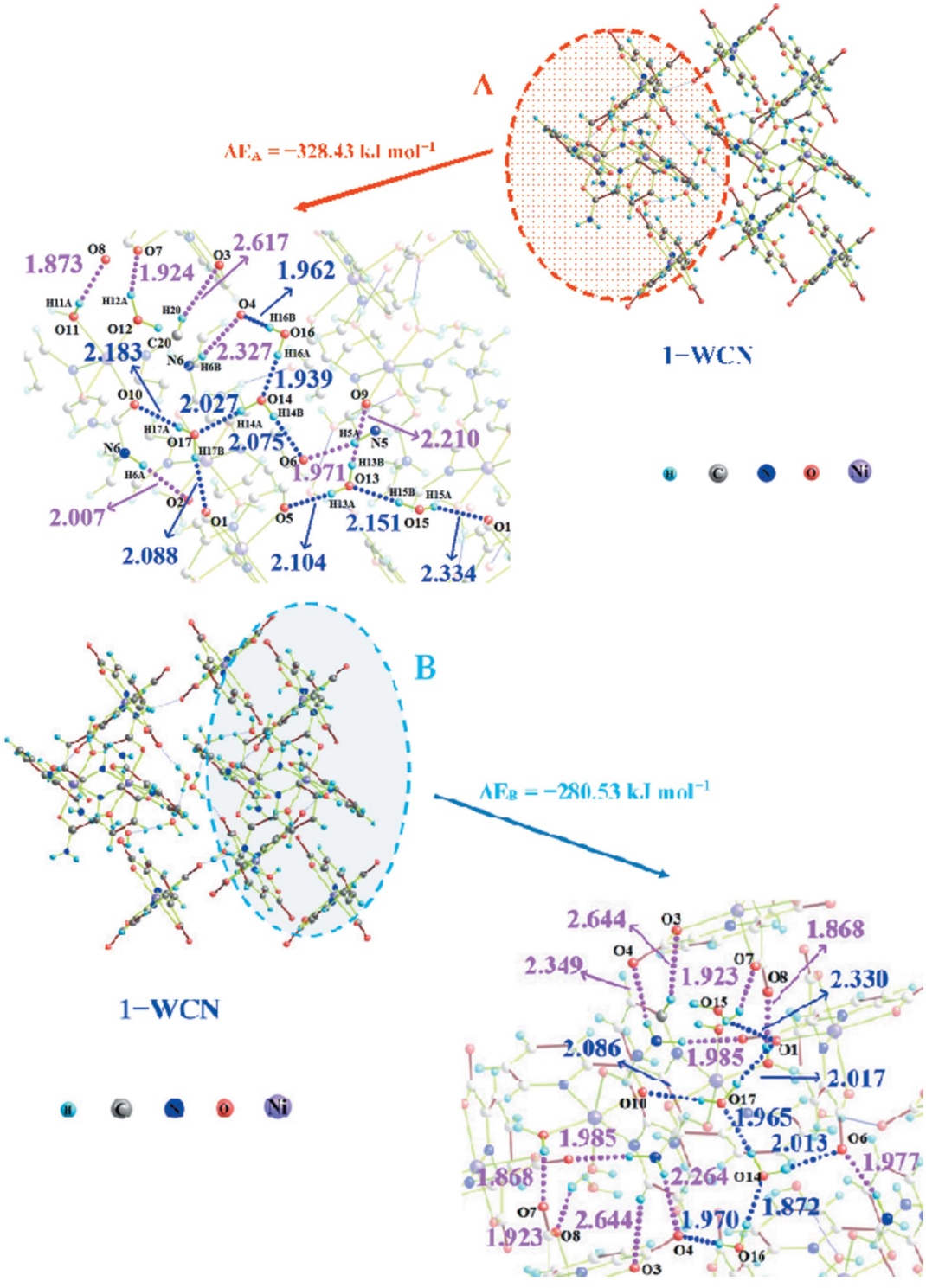

Figure 8
The optimized **1-WCN** constructed by hydrogen bond. For more clarity the involved hydrogen bonds are shown in two separated parts A and B. The pure water clustered bonds highlighted in blue dots. Distances are shown in Å.

Table 2
Selected experimental and optimized B3LYP/LANL2DZ/6-311+G(d,p) atomic distances (Å) and angles (°) for **1-mon**.

$C_{26}H_{31.34}N_6Ni_2O_{16.67}$

	Experimental	Calculated		Experimental	Calculated		Experimental	Calculated
Ni1—O1	2.1552 (17)	1.988	N2—Ni1—O3	106.11 (7)	95.06	N3—Ni2—O10	91.79 (7)	95.86
Ni1—N1	1.9586 (19)	1.883	O3—Ni1—O5	96.05 (7)	90.95	N4—Ni2—O10	78.81 (7)	83.20
Ni1—O5	2.1286 (17)	1.955	N1—Ni1—O1	76.99 (7)	84.63	O9—Ni2—N3	79.87 (7)	86.80
Ni2—O9	2.0775 (17)	1.998	N1—Ni1—O5	101.74 (7)	94.71	O9—Ni2—N4	97.93 (7)	92.94
Ni2—O11	2.0292 (18)	2.005	O1—Ni1—O5	91.62 (7)	89.77	O11—Ni2—N3	97.31 (8)	94.27
Ni2—O12	2.0759 (16)	1.987	O1—Ni1—O7	93.88 (7)	89.88	N3—Ni2—O12	90.64 (7)	90.92
Ni2—N3	2.064 (2)	1.926	O5—Ni1—N2	77.95 (7)	85.44	N4—Ni2—O12	91.73 (7)	90.85
Ni2—N4	2.064 (2)	1.933	O7—Ni1—N2	77.33 (7)	85.45	N1—Ni1—O5—C8	170.32 (17)	179.61
O1—Ni1—O3	155.18 (7)	170.02	O9—Ni2—O12	170.23 (7)	170.54	O3—Ni1—O1—C1	−9.2 (3)	−5.30
O5—Ni1—O7	155.21 (7)	165.21	N3—Ni2—N4	170.44 (8)	176.36	N4—Ni2—N3—C20	101.27 (1)	124.52
N1—Ni1—O3	78.35 (7)	85.40	O10—Ni2—O12	93.68 (7)	93.65	O10—Ni2—N3—C20	91.26 (6)	88.20

bonding capabilities of the various Ni^{II} cations, the crystal packing in the structures cited varies considerably. However, many contain uncoordinated water molecules which play important roles in the 3D structures and in at least one (QOCPAA) the presence of 'water clusters' is also noted.

The layers are connected by O11—H11*B*···O16, O16—H16*A*···O14, O16—H16*B*···O4 and O17—H7*B*···O10 hydrogen bonds (Fig. 4).

3.2. Theoretical studies on 1W

As an entry into our theoretical studies, two calculated monomer structures, **1-mon** and **1W-mon**, for studying the solid state networks are considered. The selected geometrical parameters show reasonable agreement between the experimental and optimized structures (Table 2). However, where there are significant differences in parameters between experimental and optimized structures it is because of ignoring any symmetry constraints during optimization. The largest variations are in the Ni1—O3 and Ni1—O1 bond lengths, O1—Ni1—O3 bond angle and N4—Ni2—N3—C20 torsion angle with differences of 0.182 and 0.164 Å and 14.75° and 23.25°, respectively. In contrast, the smallest differences are seen for Ni2—O11 (0.24 Å) and O10—Ni2—O12 (0.3°). We suggest that the water molecules positioned near **1-pydc** (bearing Ni1) make a strong intermolecular hydrogen bond with the oxygen atoms of a carboxylate moiety (see Section 3.3) so that ignoring some or all of these water molecules in the optimized structures can explain these discrepancies as most of the optimized hydrogen bonds to the uncoordinated water molecules are stronger and shorter than the corresponding experimental bonds (see Table 2). These strong hydrogen bonds turn **1-pydc** and **1-pycm** close to each other to form O12—H12*B*···O2 (1.414 Å) in optimized **1-mon**. More notable is the cluster of three hydrogen bonds (WCHBs) in the optimized structure of **1W-mon**, namely, O12—H12*B*···O13—H13*A*···O14—H14*B*···O2 (H12*B*···O13 = 1.082, H13*A*···O14 = 1.097 and H14*B*···O2 =

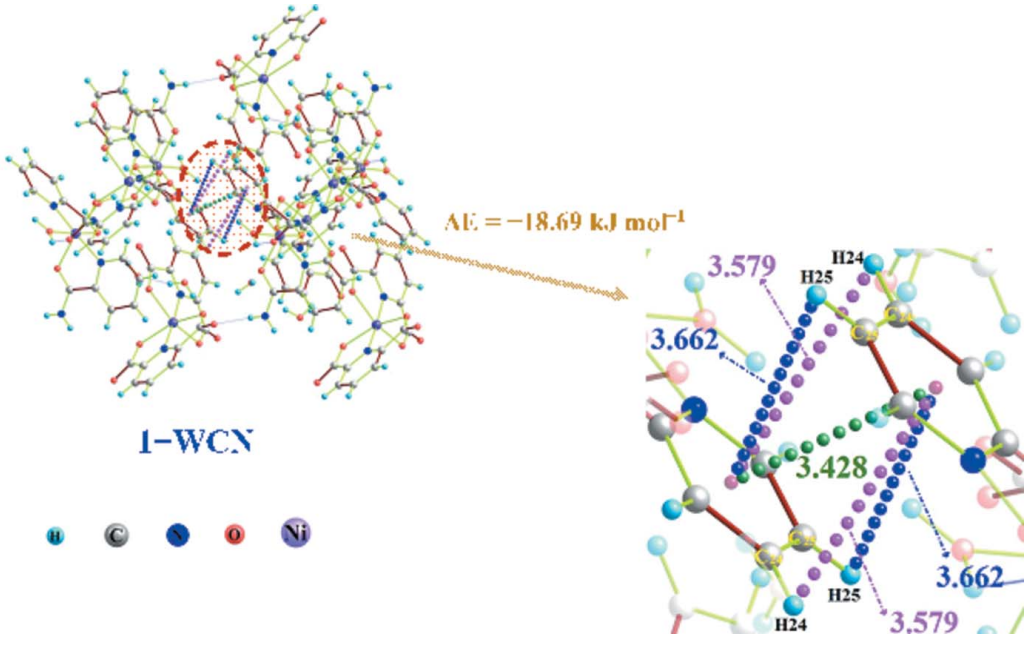

Figure 9
The optimized **1-WCN** constructed by stacking interactions. Distances are shown in Å.

Table 3
Values of the density of all electrons $\rho(\mathbf{r})$, Laplacian of electron density $\nabla^2(\mathbf{r})$, potential energy density $V(\mathbf{r})$ and Lagrangian kinetic energy $G(\mathbf{r})$ (in Hartree) at the bond critical points (3, −1), for the noncovalent interactions in **1-CN** and their respective energies E_{int} (kJ mol^{-1}) defined by two methods.

Interaction	$\rho(\mathbf{r})$	∇^2(r)	$V(\mathbf{r})$	$G(\mathbf{r})$	$E_{int} = -V(\mathbf{r})/2$ (Espinosa *et al.*, 1998)	$E_{int} = 0.429G(\mathbf{r})$ (Vener *et al.*, 2012)
O11—H11*A*···O8	0.024748	0.108412	−0.022282	0.026698	29.25	30.07
O12—H12*A*···O7	0.020573	0.097225	−0.021574	0.025144	28.32	29.24
O11—H11*A*···O8	0.024571	0.108571	−0.021208	0.024718	27.84	28.63
N5—H5*A*···O6	0.022125	0.105294	−0.015815	0.018432	20.76	21.79
N6—H6*A*···O2	0.017630	0.012304	−0.014634	0.017056	19.21	20.47
N5—H5*B*···O8	0.012403	0.070507	−0.013164	0.015342	17.28	18.10
N5—H5*B*···O8	0.012170	0.069189	−0.012714	0.014818	16.69	17.52
N6—H6*B*···O4	0.008153	0.050724	−0.012364	0.014410	16.23	17.39
C17—H17···O8	0.003896	0.027512	−0.007275	0.008479	9.55	10.38
C17—H17···O8	0.004184	0.028865	−0.006330	0.007378	8.31	9.57
C23—H23···O4	0.002933	0.021303	−0.005614	0.006543	7.37	8.02
N5—H5*B*···π(pyridine)	0.001775	0.012005	−0.003855	0.004493	5.06	6.49
N5—H5*A*···π(pyridine)	0.001715	0.010221	−0.003260	0.003800	4.28	5.13
C24—H24···π(pyridine)	0.003044	0.015719	−0.002400	0.002797	3.15	4.42
C10—H10···π(pyridine)	0.001713	0.010217	−0.002148	0.002504	2.82	3.61
C25—H25···π(pyridine)	0.002964	0.015462	−0.002042	0.002379	2.68	3.77
π(pyridine)···π(pyridine)	0.001659	0.009327	−0.001653	0.001927	2.17	2.64

Table 4
Values of the density of all electrons $\rho(\mathbf{r})$, Laplacian of electron density $\nabla^2(\mathbf{r})$, potential energy density $V(\mathbf{r})$ and Lagrangian kinetic energy $G(\mathbf{r})$ (in Hartree) at the bond critical points (3, −1) for the noncovalent interactions in **1-WCN** and their respective energies; E_{int} (kJ mol^{-1}) defined by two methods.

Interaction	$\rho(\mathbf{r})$	$\nabla^2(\mathbf{r})$	$V(\mathbf{r})$	$G(\mathbf{r})$	$E_{int} = -V(\mathbf{r})/2$ (Espinosa *et al.*, 1998)	$E_{int} = 0.429G(\mathbf{r})$ (Vener *et al.*, 2012)
O11—H11*A*···O8	0.024274	0.113265	−0.021680	0.025872	28.46	29.14
O16—H16*A*···O14	0.023927	0.104591	−0.020774	0.024798	27.27	27.93
O11—H11*A*···O8	0.023651	0.098727	−0.020591	0.024727	27.03	27.85
O12—H12*A*···O7	0.023395	0.103742	−0.020027	0.023937	26.29	26.96
O16—H16*A*···O14	0.023046	0.098390	−0.019303	0.023235	25.34	26.17
O16—H16*B*···O4	0.022830	0.092672	−0.018245	0.021823	23.95	24.58
O14—H14*A*···O17	0.022638	0.097420	−0.017909	0.021593	23.51	24.32
O16—H16*A*···O14	0.022389	0.098724	−0.017734	0.021175	23.28	23.85
O14—H14*B*···O6	0.021982	0.089539	−0.016653	0.020128	21.86	22.67
O17—H17*B*···O1	0.021473	0.088736	−0.016203	0.019355	21.27	21.80
O14—H14*A*···O17	0.020471	0.082640	−0.015898	0.019275	20.87	21.71
O14—H14*B*···O6	0.019766	0.082354	−0.015350	0.018609	20.15	20.96
O17—H17*A*···O10	0.019287	0.085297	−0.015068	0.018121	19.78	20.41
O17—H17*B*···O1	0.018864	0.081555	−0.014725	0.017713	19.33	19.95
O13—H13*A*···O5	0.016528	0.079534	−0.014443	0.017571	18.96	19.79
O15—H15*B*···O13	0.015820	0.078342	−0.013895	0.016745	18.24	18.86
O17—H17*A*···O10	0.014392	0.076234	−0.013628	0.016541	17.89	18.63
O13—H13*B*···O9	0.012537	0.074329	−0.012280	0.014960	16.12	16.85
O15—H15*A*···O1	0.009745	0.073227	−0.011221	0.013842	14.73	15.59
N5—H5*A*···O6	0.012429	0.054238	−0.013384	0.016221	17.57	18.27
N5—H5*A*···O6	0.010534	0.052234	−0.012409	0.015085	16.29	16.99
N6—H6*A*···O2	0.008721	0.057647	−0.011907	0.014472	15.63	16.30
N6—H6*A*···O2	0.007358	0.053396	−0.011290	0.013966	14.82	15.73
N6—H6*B*···O4	0.006822	0.052275	−0.010825	0.013424	14.21	15.12
N6—H6*B*···O4	0.004326	0.049873	−0.010513	0.013016	13.80	14.66
C20—H20···O3	0.003737	0.018498	−0.007054	0.008763	9.26	9.87
C20—H20···O3	0.002589	0.019923	−0.006666	0.008301	8.75	9.35
C24—H24···π(pyridine)	0.001893	0.013738	−0.002011	0.003001	2.64	3.38
C25—H25···π(pyridine)	0.001625	0.012785	−0.01577	0.002521	2.07	2.84
π(pyridine)···π(pyridine)	0.001472	0.009531	−0.001356	0.002122	1.78	2.39

1.648 Å). Beside this a new N6—H6*B*···O2 (2.065 Å) interaction with WCHBs generates a bifurcated N6—H6*B*···O2···H14*B*—O14 hydrogen bond (H6*B*···O2 = 2.065 and O2···H14*B* = 1.648 Å) which increases the links between the cation and anion (see Fig. 5).

3.3. Full DFT consideration of 3D network packed by noncovalent interactions

The above-mentioned monomers are self-assembled by intermolecular noncovalent forces to form the appropriate

crystalline networks marked **1-CN** and **1-WCN**. Over the last decade, the energies of these noncovalent interactions have been successfully estimated using precise DFT-D calculations (Chahkandi & Rahnamaye Aliabad, 2019; Chahkandi *et al.*, 2017; Chahkandi, 2016; Yunus *et al.*, 2016; Eshtiagh-Hosseini Mirzaei *et al.*, 2013; Mirzaei *et al.*, 2012; Seth *et al.*, 2011). The dispersion correction implemented in B3LYP-D for optimization of selected 3D networks has also been described (Jurečka *et al.*, 2007). In order to study the role of water molecules in the stabilization of the supramolecular structure, we generated two model networks, *with* and *without* uncoordinated water molecules, from **1-mon** and **1W-mon** which are designated as **1-CN** and **1-WCN**, respectively (see Figs. 6, 7, 8 and 9). The latter includes two water molecules to supply the minimum number of essential noncovalent interactions for **1-WCN** (Figs. 8 and 9). The structural comparison of these optimized networks presents some means of assessing the role of the outer-sphere water in the stability of water clusters in the packing. Complementary to Sections 3.1 and 3.2, there is an obvious chain of O—H···O and N—H···O hydrogen bonds connecting two Ni complexes in **1 W-mon**. Comparison of the related experimental (Exp.) and calculated (Calcd) water hydrogen bond as N6—H6*B*···O2 (Exp. = 2.035, Calcd = 2.065 Å), O14—H14*B*···O2 (Exp. = 2.048, Calcd = 1.948 Å), O13—H13*A*···O14 (Exp. = 1.918, Calcd = 1.797 Å), and O12—H12*B*···O13 (Exp. = 2.173, Calcd = 1.982 Å) shows a greater stabilization of the latter over the experimental structure of 131.52 kJ mol^{-1}. However, the observed different structural parameters between experimental and optimized structures are because of ignoring any symmetry constraints during optimization. A detailed description of the noncovalent interactions considers the optimized **1-CN** structure as a pentamer of **1-mon** containing five $[Ni(2,6\text{-pydc})_2]^{2-}$ (**Ni-pydc**) and five $[Ni_2(py\text{-}2\text{-}cm)_2]^{2+}$ (**Ni-pycm**) complexes webbed through different N—H···O, O—H···O and C—H···O hydrogen bonds and N—H···π, C—H···π and π···π stacking interactions. Actually, in the selected networks (**1-CN** and **1-WCN**) some C—H···O hydrogen bonds were found which, in the optimized structures, have C—H···O angles ranging from 145 to 167° but because the H···O distances are long, they have low binding energies (totally structural studies of all involved interactions are given in Table 1S). Moreover, it is interesting that for some connectivities in the monomer and network structures there is more than one bond distance value. For example, in **1-CN** there are N6—H6*B*···O2 (Exp. = 2.035, Calcd = 2.065 and 2.353 Å) and N5—H5*B*···O8 (Exp. = 2.157, Calcd = 2.164 and 2.171 Å), but in **1-WCN**, O15 participates in two hydrogen bonds as O15—H15*B*···O13 (Exp. = 2.166, Calcd = 2.151) and O15—H15*A*···O1 (Exp. = 2.295, Calcd = 2.334).

As delineated in Fig. 6, one of every N5—H5*B*···O8 (2.164 Å), O11—H11*A*···O8 (1.965 Å), C17—H17···O8 (2.661 Å), O12—H12*A*···O7 (1.992 Å), C23—H23···O4 (2.787 Å), N6—H6*B*···O4 (2.353 Å) and N6—H6*A*···O2 (1.996 Å) (assigned as Part A), and one of each O12—H12*A*···O7 (1.922 Å), O11—H11*A*···O8 (1.893 Å), C23—H23···O4 (2.787 Å), N6—H6*B*···O4 (2.353 Å), N5—H5*B*···O8 (2.171 Å) and C17—H17···O8 (2.647 Å), and a double set of N5—H5*A*···O6 (1.937 Å) (assigned as Part B) hydrogen bonds give a calculated stabilization energy of $\Delta E_{HBCN} = -294.41$ kJ mol^{-1}. Moreover, the oriented stacking interactions as shown in three separated parts as a double set of each N5—H5*A*···π(py) (3.970 Å), N5—H5*B*···π(py) (3.669 Å) (assigned as Part A), a double set of each C25—H25···π(py) (3.976 Å), C24—H24···π(py) (3.822 Å), and a π(py)···π(py) (3.428 Å) (assigned as Part B), and Part C as one double set of C10—H10···π(py) (3.917 Å) interactions contribute $\Delta E_{StackCN} = -49.77$ kJ mol^{-1} to the stabilization of **1-CN** (Fig. 7 and Table 1S). In the second model network, **1-WCN** (containing six **Ni-pydc**, four **Ni-pycm** and nine water molecules), the numerous strong O—H···O WCHBs have significantly firmed up the interwoven organization of the monomer complexes. The water molecules separate the monomers by the formation of additional hydrogen bonds so that few stacking interactions compared with **1-CN** can be found. The blue colored bonds show the full development of water hydrogen bonds consisting of O15—H15*B*···O13 (2.151 Å), O13—H13*A*···O5 (2.104 Å), and pairs of O17—H17*B*···O1 (2.088 and 2.017 Å), O14—H14*B*···O6 (2.075 and 2.013 Å), O14—H14*A*···O17 (2.027 and 1.965 Å), O16—H16*A*···O14 (1.939 and 1.872 Å), O16—H16*B*···O4 (1.962 and 1.970 Å), O17—H17*A*···O10 (2.183 and 2.086 Å), and pairs of O15—H15*A*···O1 (2.334 and 2.330 Å). For clarity, hydrogen bonds (see detailed structure in Fig. 8) and stacking interactions (see Fig. 9) have been illustrated separately with each type stabilizing the network by 608.96 and 18.79 kJ mol^{-1}, respectively, with 487.91 kJ mol^{-1} (more than 77%) of the calculated energy associated with the O—H···O WCHBs. It is thus evident that the stronger and more plentiful hydrogen bonds, especially the stronger O—H···O ones dominate the stabilization and packing design of the crystalline network (*cf.* Table 1S and Figs. 6, 7, 8 and 9).

One should not overlook the interplay of all pertinent interactions if one wishes an accurate measure of binding and stabilization energies of related bonds and crystalline networks. In a generic *D*—H···*A* interaction (hydrogen bond or stacking), if one terminal atom concurrently contributes to more than one hydrogen bond bearing antithetic characters (Lewis base and acid), that interaction would be reinforced (*cf.* type 1 above).

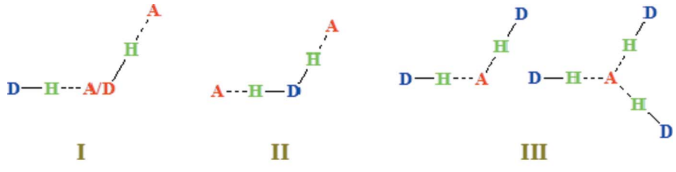

Scheme 1

On the other hand, hydrogen bonds characterized as types II and III will result in progressively weaker interactions (Chahkandi *et al.*, 2017; Yunus *et al.*, 2016; Chahkandi & Rahnamaye Aliabad, 2019; Mirzaei *et al.*, 2012; Eshtiagh-Hosseini, Chahkandi *et al.*, 2013; Chahkandi, 2016; Eshtiagh-Hosseini, Mirzaei *et al.*, 2013; Seth *et al.*, 2011). Therefore, different forces affecting particular O—H···O WCHBs in

these structures shape the resulting network as will be discussed. There are some weakening effects in **1-CN** between N5—H5*B*···O8 (2.164 Å), O11—H11*A*···O8 (1.965 Å), and C17—H17···O8 (2.661 Å) and between C23—H23···O4 (2.787 Å) and N6—H6*B*···O4 (2.353 Å) with the same oxygen-acceptor site which weaken each other and show elongation in comparison with the experimental values. In addition, considerable weakening effects in the stacking interactions N5—H5*A*···π(py) (3.970 Å) and N5—H5*B*···π(py) (3.669 Å) and also C25—H25···π(py) (3.976 Å) and C24—H24···π(py) (3.822 Å) having the same acceptor Lewis base site were seen (see Fig. 7 and Table 1S).

The interesting interplaying effects between water molecules chained through clustered O—H···O interactions in **1-WCN** can be seen in that some of them partake in bifurcated hydrogen bonds. The selected structure of the network is made up of nine water molecules, two groups of three mutually hydrogen-bonded molecules, a pair of hydrogen-bonded molecules and one water molecule without any connection to the above groups. The two groups of three water molecules hydrogen bond with the carboxylic group of 2,6-pydc and the carboxamide of py-2-cm. [For clarity they are depicted separately (A and B) and highlighted in blue, see Fig. 8.] There are weakening effects between O15—H15*A*···O1 and O15—H15*B*···O13 hydrogen bonds and a cooperative one between the later and a O13—H13*A*···O5 bond length elongation 0.039 Å, shrinkages of 0.015 Å and 0.062 Å, and elongation of 0.035 Å, respectively. These periodic countertype effects can be also found in the triple handles of clustered uncoordinated water molecules. These are O16—H16*B*···O4 and O16—H16*A*···O14 with weakening, cooperativeness of O16—H16*A*···O14 with O14—H14*A*···O17 and O14—H14*B*···O6, but weakening of O14—H14*A*···O17 and O14—H14*B*···O6, and eventually coaction of O14—H14*A*···O17 with O17—H17*A*···O10 and O17—H17*B*···O1, simultaneously. The same situation is found for the clustered water hydrogen bond and is marked as Part B in Fig. 8. It can be noted that the three bifurcated O16—H16*B*···O4···H6*B*—N6, O14—H14*B*···O6···H5*A*—N5, and O17—H17*B*···O1···H15*A*—O15 hydrogen bonds are interesting in that the two hydrogen bonds contained in each bifurcated system weaken each other (*cf*. experimental bond value and optimized ones in Table 1S). In summary, all of these effects for constructing the network stabilize **1-CN** and **1-WCN** by 344.18 and 627.75 kJ mol^{-1}, respectively.

3.4. Atoms in molecules

There are four critical points (CPs) marked as (3, −3), (3, −1), (3, +1) and (3, +3) with that designated as (3, −1) having the maximum value of electron density [ρ(**r**)] at bond distance (r_c) placed in the plane defined by Cartesian axes. The results of the QTAIM analysis show the existence of BCPs in the optimized structures of **1-CN** and **1-WCN** which correspond to all the hydrogen bonds and π···stacking interactions considered above (Bader, 1990, 1985, 1991). The low calculated values of ED (0.024800−0.001480 Hartree) and Laplacian positive quantity (0.108600−0.009330 Hartree) indicate the generic noncovalent interactions agree with previous studies (Chahkandi & Rahnamaye Aliabad, 2019; Bohórquez *et al.*, 2011; Bader, 1990, 1985, 1991). The energy data were measured based on prior methodology (Espinosa *et al.*, 1998; Vener *et al.*, 2012) (30.1−2.7 kJ mol^{-1}) (Tables 3 and 4). The first research team suggested that the parity of Lagrangian kinetic energy G(**r**) and potential energy density V(**r**) at BCPs indicates the desired interactions. Namely, noncovalent interactions correspond to the ratio $-G(\mathbf{r})/V(\mathbf{r}) > 1$ but covalent bonds have $-G(\mathbf{r})/V(\mathbf{r}) < 1$ and these agree with the results in Tables 3 and 4. Generally, a stronger interaction has higher ED and Laplacian values which lead to higher calculated potential and Lagrangian kinetic energy absolute values, which is consistent with O—H···O and N—H···O hydrogen bonds being the strongest intermolecular interactions (*cf*. Tables 3 and 4, and 1S). For example, O11—H11*A*···O8 in both structures of **1-CN** and **1-WCN** shows maximum electron density and Laplacian values as the strongest ones that has consistency with those obtained data of interactions binding energies from DFT-D calculations. Moreover, the energies obtained using the Espinosa (Espinosa *et al.*, 1998) and Vener (Vener *et al.*, 2012) formula agree well with those obtained from calculations of binding energy (*cf*. Table 1S and Tables 3 and 4). All of these contacts can be found in the optimized network structures of **1–CN** and **1–WCN**; the small red, yellow, and green dots represent the BCPs, RCPs and the cage CPs, respectively (see completed data in Figs. 2S and 3S and Tables 3 and 4). For clarity, just a part of the WCHBs of **1-WCN** have been marked in Fig. 3S. The topological AIM results are consistent with the calculated stabilization energies showing that hydrogen bonds are more important in stabilizing the crystalline network than π···stacking interactions (*cf*. Tables 1S, 3 and 4).

4. Conclusion

In this work, the title compound is composed of a mononuclear complex cation and a mononuclear complex anion of Ni^{II} bearing pyridine-2-carboxamide (py-2-cm) and pyridine-2,6-dicarboxylic ligands, $[Ni\{2\text{-}H_2NC(=O)C_5H_4N\}_2(H_2O)_2][Ni\{2,6\text{-}(O_2C)_2C_5H_3N\}_2]\cdot 4.67H_2O$. Its structure was characterized by single crystal X-ray diffraction. For a greater understanding of the role of water molecules in the X-ray crystal structure, particularly the role of water clusters interactions, two model crystalline networks, one without the cluster of water molecules (labeled as 1-CN) and one with it (the experimental one; 1-WCN) were discussed, in detail. The optimized DFT-D-B3LYP/6-311+G(d,p) structures of **1W-mon**, **1-CN**, and **1-WCN** show that O—H···O, N—H···O, C—H···O and C—H···N hydrogen bonds, and C—H···π, N—H···π and π···π stacking interactions stabilize the crystalline 3D network. The calculated energetic results obtained from DFT-D and AIM computations indicate that hydrogen bonds govern the formation of the networks in the following order of importance: O—H···O > N—H···O > C—H···O >, N—H···π > C—H···π > π···π.

Acknowledgements

MC gratefully acknowledges the financial support by the Hakim Sabzevari University, Sabzevar, Iran. MM acknowledges financial support from Ferdowsi University of Mashhad. MM is also supported by the Iran Science Elites Federation and Zeolite and Porous Materials Committee of Iranian Chemical Society. The authors wish to thank the co-editor for helpful discussions.

Funding information

The following funding is acknowledged: Ferdowsi University of Mashhad.

References

Bader, R. F. W. (1985). *Acc. Chem. Res.* **18**, 9–15.
Bader, R. F. W. (1990). In *Atoms in Molecules: A Quantum Theory*. Oxford: Clarendon Press.
Bader, R. F. W. (1991). *Chem. Rev.* **91**, 893–928.
Belda, O. & Moberg, C. (2005). *Coord. Chem. Rev.* **249**, 727–740.
Bohórquez, H. J., Boyd, R. J. & Matta, C. F. (2011). *J. Phys. Chem. A*, **115**, 12991–12997.
Boys, S. B. & Bernardi, F. (1970). *Mol. Phys.* **19**, 553–566.
Bruker (2016). *APEX2*, *SADABS*, *SAINT* and *SHELXTL*, Bruker-AXS, Madison, WI, USA.
Carlucci, L., Ciani, G. & Proserpio, D. M. (2003). *Coord. Chem. Rev.* **246**, 247–289.
Castro, R. A. E., Ribeiro, J. D. B., Maria, T. M. R., Ramos Silva, M., Yuste-Vivas, C., Canotilho, J. & Eusébio, M. E. S. (2011). *Cryst. Growth Des.* **11**, 5396–5404.
Chahkandi, M. (2016). *J. Mol. Struct.* **1111**, 193–200.
Chahkandi, M. & Rahnamaye Aliabad, H. A. (2019). *Chem. Phys.* **525**, 110418–110427.
Chahkandi, M., Bhatti, M. H., Yunus, U., Shaheen, S., Nadeem, M. & Tahir, M. N. (2017). *J. Mol. Struct.* **1133**, 499–509.
Deng, Z.-P., Huo, L.-H., Li, M.-S., Zhang, L.-W., Zhu, Z.-B., Zhao, H. & Gao, S. (2011). *Cryst. Growth Des.* **11**, 3090–3100.
Desiraju, G. R. (2003). *Crystal Design: Structure and Function* (*Perspectives in Supramolecular Chemistry*). Chichester: Wiley.
Eshtiagh-Hosseini, H., Aghabozorg, H., Mirzaei, M., Amini, M. M., Chen, Y.-G., Shokrollahi, A. & Aghaei, R. (2010). *J. Mol. Struct.* **973**, 180–189.
Eshtiagh-Hosseini, H., Chahkandi, M., Housaindokht, M. R. & Mirzaei, M. (2013). *Polyhedron*, **60**, 93–101.
Eshtiagh-Hosseini, H., Mirzaei, M., Biabani, M., Lippolis, V., Chahkandi, M. & Bazzicalupi, C. (2013). *CrystEngComm*, **15**, 6752–6768.
Espinosa, E., Molins, E. & Lecomte, C. (1998). *Chem. Phys. Lett.* **285**, 170–173.
Farrugia, L. J. (1997). *J. Appl. Cryst.* **30**, 565.
Farrugia, L. J. (1999). *J. Appl. Cryst.* **32**, 837–838.
Frisch, M. J. *et al.* (2009). *GAUSSIAN09*, revision A.02. Gaussian, Inc.: Wallingford, CT, USA.
Groom, C. R., Bruno, I. J., Lightfoot, M. P. & Ward, S. C. (2016). *Acta Cryst.* B**72**, 171–179.
He, J., Tan, G. P., Zhang, J. X., Zhang, Y. N. & Yin, Y. G. (2008). *Inorg. Chem. Commun.* **11**, 1094–1096.
Jerome, P., Bhuvanesh, N. S. P. & Karvembu, R. (2016). *Zh. Strukt. Khim.* **57**, 528–533.
Jurečka, P., Černý, J., Hobza, P. & Salahub, D. R. (2007). *J. Comput. Chem.* **28**, 555–569.
Kawamoto, T., Hammes, B. S., Ostrander, R., Rheingold, A. L. & Borovik, A. S. (1998). *Inorg. Chem.* **37**, 3424–3427.
Kim, Y.-J., Kwak, H., Lee, S. J., Lee, J. S., Kwon, H. J., Nam, S. H., Lee, K. & Kim, C. (2006). *Tetrahedron*, **62**, 9635–9640.
Kirillova, M. V., Kirillov, A. M., Guedes da Silva, M. F. C., Kopylovich, M. N., Fraústo da Silva, J. J. R. & Pombeiro, A. J. L. (2008). *Inorg. Chim. Acta*, **361**, 1728–1737.
Lee, S. H., Han, J. H., Kwak, H., Lee, S. J., Lee, E. Y., Kim, H. J., Lee, J. H., Bae, C., Lee, S. N., Kim, Y. & Kim, C. (2007). *Chem. Eur. J.* **13**, 9393–9398.
Leroy, C., Johannson, R. & Bryce, D. L. (2019). *J. Phys. Chem. A*, **123**, 1030–1043.
Lin, X.-M., Chen, L., Fang, H.-C., Zhou, Z.-Y., Zhou, X.-X., Chen, J.-Q., Xu, A.-W. & Cai, Y.-P. (2009). *Inorg. Chim. Acta*, **362**, 2619–2626.
Liu, B.-X., Yu, Y.-P., Cao, Z. & Zhang, L.-J. (2009). *Acta Cryst.* E**65**, m277–m278.
Lumb, I., Sran, B. S., Sood, H., Arora, D. S. & Hundal, G. (2017). *Polyhedron*, **127**, 153–166.
Macrae, C. F., Sovago, I., Cottrell, S. J., Galek, P. T. A., McCabe, P., Pidcock, E., Platings, M., Shields, G. P., Stevens, J. S., Towler, M. & Wood, P. A. (2020). *J. Appl. Cryst.* **53**, 226–235..
Mashhadi, S. M. A., Yunus, U., Bhatti, M. H. & Tahir, M. N. (2014). *J. Mol. Struct.* **1076**, 446–452.
McMurtrie, J. & Dance, I. (2010). *CrystEngComm*, **12**, 3207–3217.
Mirzaei, M., Aghabozorg, H. & Eshtiagh-Hosseini, H. (2011). *J. Iran. Chem. Soc.* **8**, 580–607.
Mirzaei, M., Eshtiagh-Hosseini, H., Chahkandi, M., Alfi, N., Shokrollahi, A., Shokrollahi, N. & Janiak, A. (2012). *CrystEngComm*, **14**, 8468–8484.
Mirzaei, M., Eshtiagh-Hosseini, H., Lippolis, V., Aghabozorg, H., Kordestani, D., Shokrollahi, A., Aghaei, R. & Blake, A. J. (2011). *Inorg. Chim. Acta*, **370**, 141–149.
Mobin, S. M., Mishra, V., Rai, D. K., Dota, K. A., Dharmadhikari, K., Dharmadhikari, J. A., Mathur, D. & Mathur, R. (2015). *Dalton Trans.* **44**, 1933–1941.
Pandey, S., Das, P. P., Singh, A. & Mukherjee, R. (2011). *Dalton Trans.* **40**, 10758–10768.
Park, H., Lough, A. J., Kim, J. C., Jeong, M. H. & Kang, Y. S. (2007). *Inorg. Chim. Acta*, **360**, 2819–2823.
Patel, R. N., Sondhiya, V. P., Patel, D. K., Shukla, K. K., Patel, D. K. & Singh, Y. (2013). *Indian J. Chem.* **52A**, 717–723
Pattabiraman, V. R. & Bode, J. W. (2011). *Nature*, **480**, 471–479.
Preez, J. G. H. du, Rohwer, H. E., van Brecht, B. J. & Caira, M. R. (1984). *J. Chem. Soc. Dalton Trans.* p. 975.
Seth, K. S., Saha, I., Estarellas, C., Frontera, A., Kar, T. & Mukhopadhyay, S. (2011). *Cryst. Growth Des.* **11**, 3250–3265.
Sheldrick, G. M. (2008). *Acta Cryst.* A**64**, 112–122.
Sheldrick, G. M. (2015). *Acta Cryst.* C**71**, 3–8.
Shi, C.-Y., Gao, E.-J., Ma, S., Wang, M.-L. & Liu, Q.-T. (2010). *Bioorg. Med. Chem. Let*, **20**, 7250–7254.
Soleimannejad, J., Moghzi, F., Hooshmand, Sh., Dankoob, Z., Ardalani, M. & Shamsipur, M. (2017). *Polyhedron*, **133**, 24–32.
Spek, A. L. (2020). *Acta Cryst.* E**76**, 1–11..
Tabatabaee, M., Amini, M. M., Saheli, S. & Vakilia, F. (2012*b*). *Acta Chim. Slov.* **59**, 375–379.
Tabatabaee, M., Tahriri, M., Tahriri, M., Ozawa, Y., Neumüller, B., Fujioka, H. & Toriumi, K. (2012*a*). *Polyhedron*, **33**, 336–340.
Tiekink, E. R. & Vittal, J. J. (2006). *Frontiers in Crystal Engineering*. Chichester: Wiley.
Tin, X.-J., Jiang, Y.-M., Wu, Z.-H. & Yu, K.-B. (2007). *Hecheng Huaxue*, **15**, 697–701.
Todd, A. & Keith, T. K. (2010). *AIM All* (Version 10.05.04). Gristmill Software, Overland Park KS, USA.

Vener, M. V., Egorova, A. N., Churakov, A. V. & Tsirelson, V. G. (2012). *J. Comput. Chem.* **33**, 2303–2309.
Yeşilkaynak, T., Özpınar, C., Emen, F. M., Ateş, B. & Kaya, K. (2017). *J. Mol. Struct.* **1129**, 263–270.
Yunus, U., Ahmed, S., Chahkandi, M., Bhatti, M. H. & Tahir, M. N. (2016). *J. Mol. Struct.* **1130**, 688–698.
Zhang, L.-J., Liu, B.-X., Ge, H.-Q. & Xu, D.-J. (2006). *Acta Cryst.* E**62**, m2180–m2182.